01 Jan 2023

Electrical Resistivity Tomography Revealing Possible Breaching Mechanism Of A Late Pleistocene Long-lasted Gigantic Rockslide Dam In Diexi, China

Lanxin Dai

Xuanmei Fan

Dan Wang

Fanyu Zhang

et. al. For a complete list of authors, see *https://scholarsmine.mst.edu/geosci_geo_peteng_facwork/2106*

Recommended Citation

L. Dai et al., "Electrical Resistivity Tomography Revealing Possible Breaching Mechanism Of A Late Pleistocene Long-lasted Gigantic Rockslide Dam In Diexi, China," *Landslides*, Springer, Jan 2023. The definitive version is available at https://doi.org/10.1007/s10346-023-02048-0

Lanxin Dai · Xuanmei Fan · Dan Wang · Fanyu Zhang · Ali P. Yunus ·
Srikrishnan Siva Subramanian · J. David Rogers · Hans-Balder Havenith

Electrical resistivity tomography revealing possible breaching mechanism of a Late Pleistocene long-lasted gigantic rockslide dam in Diexi, China

Abstract Landslide damming is a widespread phenomenon world-wide and significantly affects the evolution of fluvial landscapes. However, it is rarely witnessed from an antiquities perspective, and the case for observing their internal structure is challenging. We attempt to visualize the subsurface structure and understand the likely breaching mechanism of the late Pleistocene Diexi gigantic landslide dam (longevity of ~ 10 ka), using electrical resistivity tomography (ERT) method. Eight ERT measurements on the Diexi dam body revealed high resistivity zones near the periphery and lower resistivity zones in the middle portion of the profiles. Geomorphological mapping based on the LiDAR data determined the boundary of the landslide. Field investigation found that zones of low resistivity were connected to a ditched gully. Because breaching such an enormous lake with a total area of 21.4 km² dammed by a gigantic landslide body with intact rocks was not likely by overtopping alone. The authors postulate that differential seepage of water from the gullies through the landslide debris could have accelerated the undercutting erosion of the otherwise stable Diexi dam. Utilizing geophysical techniques, along with field geomorphology works, can provide valuable information on the evolution of a gigantic paleo-landslide dam, which has real implications for the stability evaluation and forecast of future landslide dams.

Introduction

Landslide dams are common worldwide, especially in tectonically active mountain regions. Landslide dams are defined as the permanent or ephemeral interruption of a river course by landslide deposits (Costa and Schuster 1988; Hermanns et al. 2011). The longevity of landslide dams ranges from minutes to thousands of years, depending on the volume and nature of the transposed slide debris, rates of inflow sediments and water to the lake, and rates of seepage through the blockage (Adams 1981). Breaching typically results from three types of failure processes: piping, progressive failure, and overtopping erosion (Fan et al. 2020; Wang et al. 2016). Among them, overtopping is reported as the dominant breaching cause for natural dams (91%), followed by piping/seepage (5%) and slope failures (1%) (Peng and Zhang 2012). Researchers have made enormous progress in developing landslide dam inventories, evaluating dam stability by geomorphic indices, and simulating dam-breach flood events, etc. (e.g., Dong et al. 2009; Chen and Chang 2016; Korup

2004; Meric et al. 2005; Wang et al. 2014a, 2018), see the review by Fan et al. (2020). The internal structure of landslide dams plays a key role in controlling the dam stability and breaching process, and catastrophically placed debris fields may be bereft of meaningful structural and stratigraphic exposures. It is usually difficult to characterize slide debris that is not exposed in outcrops.

In recent years, the development of advanced geophysical techniques has made it feasible to explore subsurface structures in detail, such as electromagnetic (e.g., Santamarina et al. 2005), geoelectric (e.g., Delunel et al. 2010), and seismic surveys (e.g., Havenith et al. 2018). These methods can measure the physical parameters linked with lithological, hydrological, and geotechnical characteristics of the landslides. Although they provide indirect observation, they are generally capable of characterizing the total thickness and geotechnical properties of the internal structure of geological deposits in a rapid and non-invasive manner (Korup and Tweed 2007). Based on this, many studies have utilized geophysical methods to investigate recent landslides (Perrone et al. 2014; Wang et al. 2014a, b) and monitor changes in landslide features (see a review by Whiteley et al. 2019). However, only a few dozen landslide dams have been probed or investigated by detailed geophysical surveys (see the review by Fan et al. 2021). Paleo-landslide dams are largely over-looked unless they are located within the boundaries of developed parcels that could be impacted by the reactivation of even a portion of a Paleo-landslide (Dufresne et al. 2018; Pánek et al. 2009).

It is significant to study the internal structure of paleo-landslide dams in order to better understand the mechanisms of landslide dam formation and evolution, which can also provide insights into recent and potential damming events. For example, the 1911 Sarez earthquake-induced landslide has formed the largest historic landslide dam and reservoir near Usoi, Tajikistan, which is threatening about five million people living downstream (Havenith and Bourdeau 2010). The study of paleo-landslide dams can also yield reliable and insightful results into the following challenges integral to the study of landslide dams: (1) filling the data gap of historical inventories by expanding the geological past (Costa and Schuster 1991; Fan et al. 2020; Dufresne et al. 2018); (2) understanding the predisposing factors and geomorphic processes that lead to subsequent dam failures (Korup 2002; Shen et al. 2020; Wassmer et al. 2004); (3) assessing the possible long-term geomorphic impacts and hazards (Fan et al. 2021; Strom 2010; Hewitt 2011); and (4) reconstructing the landscape evolution to Quaternary climate

change and neotectonism (Adams 1981; Hewitt 1998; King et al. 1989; Reneau and Dettier 1996; Wayne 1999; Strom 1998; Alford and Schuster 2000; Pánek et al. 2014; Břežný et al. 2021).

The discovery of ~ 30 ka B.P. old Quaternary lacustrine deposits in Diexi, eastern margin of the Tibetan Plateau, Sichuan, China, indicated the possible existence of an enormous, late Pleistocene rockslide dam (Wang et al. 2005; Wang and Meng 2008; Dai et al. 2021). Direct dating evidence advocates that the paleo-landslide dam appears to have survived more than 10,000 years in total (Wang et al. 2014b), making it indefinitely the oldest of such features within longest ever lasted (and dated) natural dam in recent geological time worldwide as per the author's know-how. Prior to the work of this article's authors, no attempts had been made to understand the internal structure of the Diexi paleo landslide dam, which made it an excellent candidate for site-specific studies to characterize the likely evolution of such features.

Reactivation of the study of such an unusual and persistent feature would be of considerable value in understanding the breaching process and failure mechanisms of landslide dams and their impacts on fluvial landscape evolution. To this end, this study investigated the Diexi paleo-landslide dam by using advanced electrical resistivity tomography (ERT), together with detailed geological and geomorphic surveys. Our studies demonstrate the nature and morphology of the paleo landslide dam and discuss the possible breaching zone and mechanism by analyzing the ERT profiles, high-resolution 3-dimensional topographic models from unmanned aerial vehicles (UAVs), and LiDAR data, as well as intense field investigations. This study demonstrates how geophysical methods could be extremely useful for revealing the internal structure of paleo-landslide dams, which could have important implications for the hazard assessment of existing and future landslide dams.

The Diexi paleo-landslide and regional geological setting

Physical evidence suggests that the Diexi paleo-landslide appears to have been formed at ~ 30 ka B.P. (Wang et al. 2005). Once-outburst flooding of the Diexi paleo dam occurred in the late Pleistocene, approximately 27 ka B.P. (Ma et al. 2018), followed by an unknown number of stable and breaching sequences. Seven fluvial terraces of different ages were identified within the lacustrine deposits. The authors hypothesize that breaching occurred several times within a time range of 20–26.5 ka ago (Wang et al. 2011). For this reason, the location of the dam body forming the lacustrine deposits is controversial, which was discussed in our previous study (Dai et al. 2021).

The landslide is located in the eastern margin of the Tibetan Plateau (Fig. 1), which is one of the most remarkable continental escarpments on earth, unveiling significant relief (~3500 m) over a short horizontal distance (~60–80 km) due to persistent tectonic uplift appurtenant to the tectonic collision of the Indian and Eurasian plates (Kirby et al. 2002). During the Mesozoic and Cenozoic Eras, the Tibetan Plateau lay within the northeastern margins of the Tethyan Himalayan domain, coincident with the growth of the Sichuan Basin along the Minshan Mountains (Chen et al. 1994; Dirks et al. 1994; Burchfiel et al. 1995; Kirby et al. 2002). The north-trend mountain range, termed Minshan Mountain, is the source of the Minjiang River, and over 60 km of it was formed by seismic erosion and recent neo-tectonism (Ma et al. 2018).

Complex geological and revolving tectonic systems are widely recognized along the Minjiang catchment. Strong neo-tectonic

zones and three major Quaternary faults were identified around these areas (Fig. 1): (1) the Minjiang Fault zone on the westernmost part, which is a north-trending and west-dipping reverse fault with a strike-slip component (Kirby et al. 2000). The northern part of Minjiang Fault extends for 85 km and is well defined. Meanwhile, it is believed that this fault extends discontinuously to the south of Jiaochang (Chen et al. 1994; Qian et al. 2000); (2) the Huya Fault bounds the Minshan mountain in the east, with a total length of approximately 60 km, which is composed of three segments. The south segment (length of 30 km) shows a combination of reverse and left-lateral movement. The middle segment associated with intense compression from the northern and southern segments produced reverse movements. The northern segment shows a left-lateral strike-slip component and may extend farther north (Chen et al. 1994; Zhang et al. 2006); (3) the Xueshan Fault is a west-trending fault that terminates against the northern side of the Minjiang fault. Kirby et al. (2000) interpreted the Xueshan Fault as playing a minor role in Cenozoic deformation observed along Minshan mountain.

One of the above three major fault zones, which likely produced strong paleo-earthquakes, is believed to have formed the Diexi gigantic landslide dam. Liquefaction patterns in the palaeo-lacustrine sediments suggest the occurrence of probably six strong earthquakes of magnitude 6–7 and one > 7, indicating intense earthquakes occurred during the period 25–20 ka B.P. (Wang et al. 2011; Zhong et al. 2019). Furthermore, in the history of recorded earthquakes, strong earthquakes with a short recurrence period are typical: September 4th, 1713 A.D. (~ M 7.5), August 25th, 1933 A.D. (M 7.5), August 16th, 1976 A.D. (M 7.2), and more than sixteen earthquakes with M 6–7 have occurred in and around Minshan mountain since the twelfth century (Fig. 1, Jiang et al. 2014; Wang and Meng 2008). Among them, the most destructive one was the M 7.5 Diexi earthquake on August 25th, 1933 A.D. During this earthquake, the paleo-Diexi gigantic landslide deposits were partly reactivated as two vast landslides, and these reactivations formed two lakes (named Xiaohaizi and Dahaizi, Fig. 2, Dai et al. 2021). The 1933 earthquake-induced landslide dams were much smaller than the Diexi paleo-landslide event. Considering the size of the paleo landslide, and evidence from geologic structures, paleoclimate studies (Jiang et al. 2014), and landslide chronologies (Wang et al. 2011), we feel that we have reason to believe that the parent Diexi paleo-landslide was most likely triggered by a paleo-earthquake.

Figures 2 and 3 illustrate the enormity of the Diexi gigantic landslide (32.0°N, 103.7°E) situated on the left bank of the Minjiang River within deeply incised V-shaped valleys. The prevailing annual weather cycle of this region exhibits a subtropical continental monsoon climate with an average temperature of 12 °C and a maximum of 32 °C. In addition, 420 mm of annual rainfall has been recorded, of which 80% occurs from May to October every year (Xu et al. 2015; Ma et al. 2018). Around the Diexi landslide, the most prominent geological feature is the Jiaochang arcuate structure (Wang et al. 2014b). It is characterized by symmetric, parallel, and parabolic structures (Fig. 2). The Jiaochang structure is cut by the left-lateral N-S striking Mingjiang Fault in the center, and three E-W striking, south-dipping reverse faults (Jiaochang, Guanchaigou, and Shidaguan faults). The 30-km-long Songpinggou fault exposed northwest of Jiaochang is N-W trending left-lateral fault. These structural zones comprise a series of Mesozoic folds and

Fig. 1 Location of the Diexi paleo-landslide, showing the major faults, historical earthquakes, and region of Fig. 2 (yellow rectangle). The upper panel shows the Eastern Tibetan, Sichuan basin, and Minjiang catchment
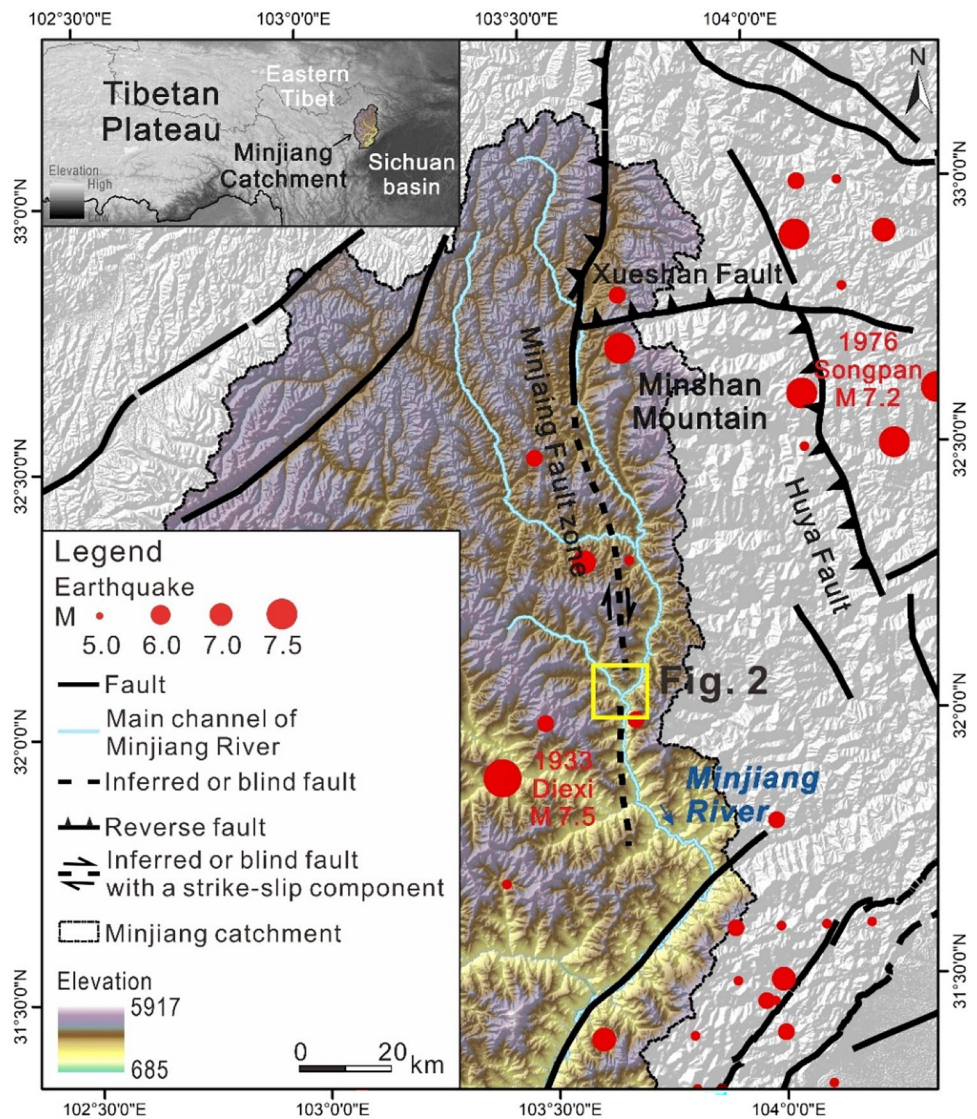
associated thrusts, suggesting that the region has under considerable compression (Ren et al. 2018; Deng et al. 2013).

The lithologies of adjacent outcrops are metamorphosed sandstone and slate of the Mid-to-Upper Triassic age units (T_2z, T_3zh), Fig. 3. The main Mesozoic strata of the Jiaochang structural zone are dominated by siliciclastic and carbonate rocks, including marble, limestone, sandstone, shale, carbonaceous phyllite, quartz-sericite-schist, and carbonatite from Devonian (Dwg_2), Carboniferous (C), Permian (P_1), and Lower Triassic (T_1b) (Wang et al. 2005; Yang et al. 2008). Quaternary sediment mainly comprises the latest Pleistocene to earliest Holocene fluvial sand and gravel deposits, Holocene soils, and colluvium (based on the geological map from the Ministry of Geology and Mineral Resources, People's Republic of China 1991). The distribution of the lacustrine deposits was little known before Dai et al. (2021), but their discovery proved the existence of the paleo-landslide dammed lake in Diexi.

Data and methods

Investigations of the Diexi gigantic landslide

Several of the co-authors flew UAVs and a helicopter equipped with LiDAR prior to the ERT survey to create high-resolution 3-dimensional topography models of the Diexi paleo-landslide dam and lake region, which were also used in our previous study on landslides triggered by the 1933 Diexi earthquake (Dai et al. 2021). The LiDAR data were acquired in 2018 with the SKYEYE SE-J1200B airborne LiDAR system configured for mountainous environments. The maximum field of view (FOV) was 50°, and the pulse rate is in the range of ~50–550 kHz. Data filtering was conducted on the TerrascanTM software and cross-checked by eye to remove any false ground data points. Finally, the acquired ground data was interpolated by constructing a TIN to derive the 0.5-m-resolution DEM. Based on this, the boundary and geomorphic features of the Diexi paleo-landslide complex were interpreted.
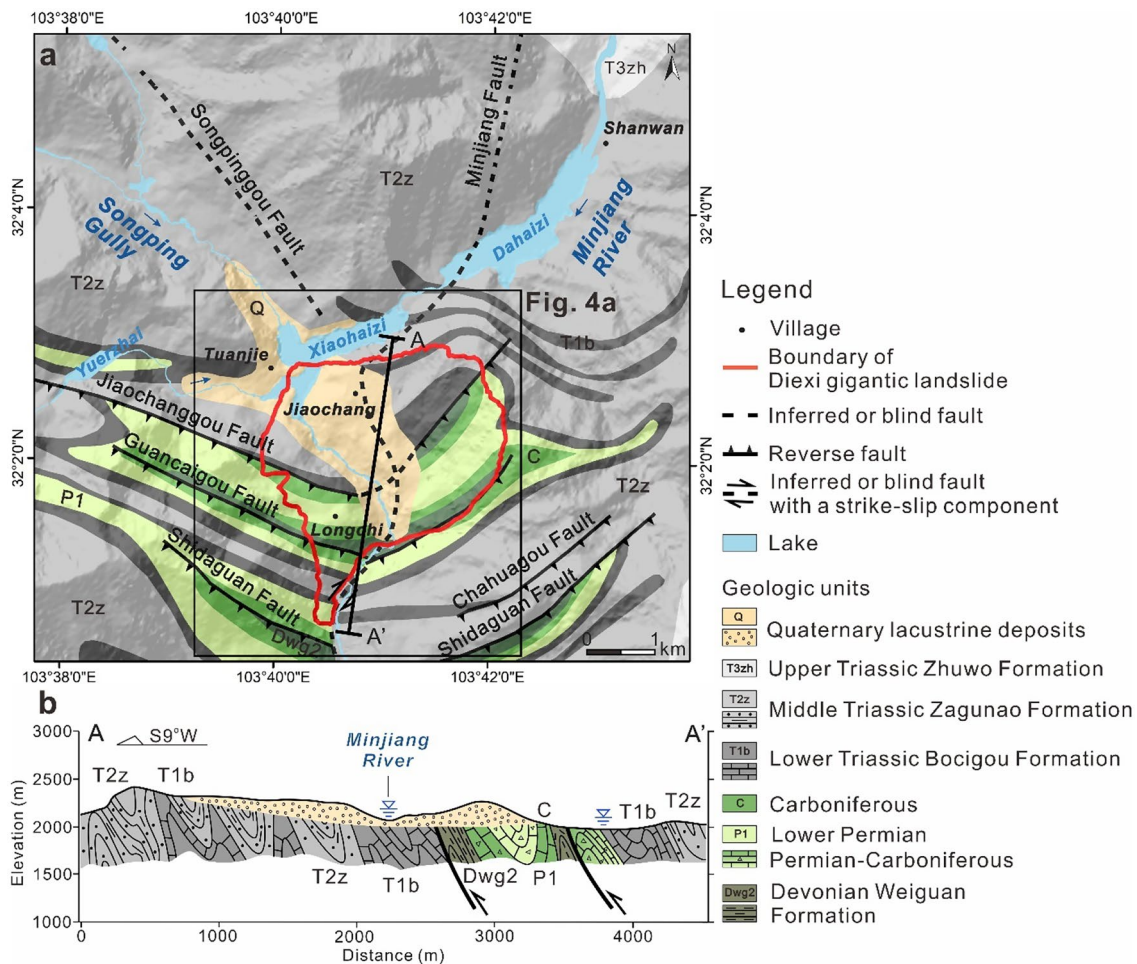
Fig. 2 a Generalized geological map of the Diexi study area (according to Fan et al. 2017), showing the localization of the paleo-landslide dam complex. The black outline marks the region of Fig. 4a; **b** geological section (A-A' in Fig. 2a) of the Jiaochang arcuate tectonic zone is based on DEMs, geological mapping (scale 1:2,000,000), and Deng et al. 2013

These fissures, including tension cracks, linear scarps, surface texture, talus, and outburst flood deposits, were confirmed by detailed field investigations. The field survey allowed the authors to select the best locations to set up the geoelectric profiles.

Investigations of the Diexi paleo-lake

To understand the stability and evolution of the Diexi paleo-landslide dam, it was important to reconstruct the areal extent of the paleo-dam formed lake. Most long-lived landslide dams preserve sedimentary archives of fluvial and lacustrine activities before catastrophic dam breaches (Fan et al. 2020). Therefore, our field investigations concentrated on the zone along the Upper Minjiang Valley and its tributary, focusing on discovering lacustrine outcrops and fluvial terraces (e.g., continuous terraces were considered to be shorelines formed along paleo-lakes (Høgaas and Longva 2019). The paleo-lake lacustrine sequences are characterized by rhythmically bedded silts, while coarse-grained rhythms composed of regularly alternating parallel sand layers represent sequences of rapid erosion and deposition (e.g., Xu et al. 2020). Individual outcrops were digitized as marked points with detailed attributes to their extent and characteristics. The LiDAR interpretation, integration of outcrop data, DEM extrapolations, and parameter calculations were evaluated using ArcGIS.

Electrical resistivity tomography

It was previously believed that the landslide deposits only existed on the left bank of the Minjiang River (the proximal side of the landslide). The right bank (distal side) did not display noticeable sedimentological features of the Diexi landslide as the result of thousands of years of evolution since its emplacement (Fig. 3b). The problem lies in distinguishing between deposits and bedrock. For this purpose, five ERT profiles (D2–D6) were carried on the distal portion, which achieved the maximum coverage possible. The proximal side, as mentioned earlier, underwent a reactivation slip during the 1933 earthquake and then was reworked for engineered construction projects, leading to some restrictions on the ground conditions for the ERT measurements. Nevertheless, two ERT profiles (D7 and D8) in this area were laid out as far as possible, to match the results of the profiles D2–D4. The ERT profile D1 was arranged in the paleo-landslide deposits where they are overlain
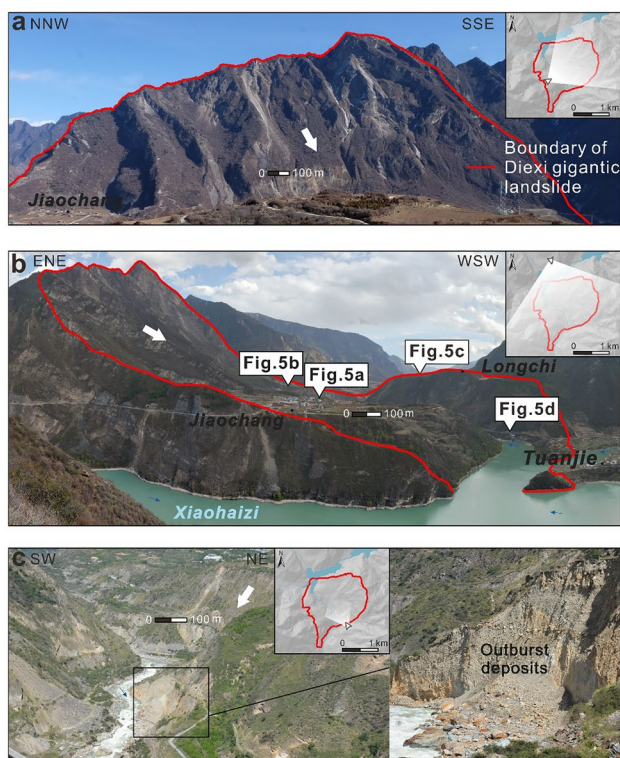
Fig. 3 The Diexi paleo-landslide complex with the boundary (the red line) and the viewing locations shown on the inserted panels. The white arrows indicate the direction of the sliding. **a** View of the head scarp taken from the summit of the paleo landslide dam (~2500 m a.s.l); **b** panoramic view from the zone of depletion to the zone of accumulation, which blocks a few gullies on the distal end. Six white boxes mark the locations where the photographs of Fig. 5 were taken; **c** views of the incised canyon formed in the landslide deposits and outburst flood deposits

by the paleo-lacustrine sediments where the terrain is most gentle. In summary, a total of eight ERT profiles were carried out in the Diexi gigantic landslide deposits, and measurement parameters and location information are presented in Table 1 and Fig. 4a, respectively. Considering the accessibility and the ground conditions, the co-author's teams set up their ERT profiles to cover the landslide

deposits at large and obtain the most considerable imaging depths possible. Our team's longest ERT profile (D1) was 1000 m long, one of the deepest and longest profiles reported in the engineering geophysical literature.

Our geophysical survey team used GeoERT IP 2401 resistivity system with an electrode spacing of 10 m in the Wenner-Schlumberger configuration. We found this configuration to be the most sensitive to changes in vertical resistivity (Dahlin and Zhou 2004). This device and array type were chosen because of the need to provide a higher signal level for deeper measurements and to reflect more sensitivity to resistivity variations with depth in the face of such a large landslide. We located these electrical profiles using a GPS and measured their topographic changes utilizing the DEM. All the measurements were performed in the dry period of the year (December) to lessen the effects of precipitation (rainwater). Resistivity data sets were inverted with the 2-D inversion algorithm of Loke and Barker (1996), which is implemented in the RES2DINV software using a smoothness-constrained least-squared method. The inversion algorithm aims to determine electrical resistivity values in a number of rectangular blocks. The block arrangement is loosely tied to data distribution in the pseudo-section to enhance the computation efficiency (Yılmaz and Narmam 2015). We then removed the topographic effect on the inverted results to reflect the true depths of the subsurface structures being profiled.

Results

The Diexi landslide dam and present-day surface morphology

The total surface area of Diexi landslide deposits covers an area of about 5.13 km². Based on the area and depth approximation from our digital elevation model, the paleo Landslide volume was estimated to be between 1.4 km³ and 2.0 km³. The travel distance of the prehistoric debris is confined by the hillslopes on the distal end (Fig. 3). The massive landslide deposits not only blocked the original Minjiang River but also blocked a few ravines/gullies on the distal end, which previously acted as a conduit for the river. One of the prominent erosion/gullies prominent has a width of over 300 m and a depth of about 100 m (marked as G2 in Figs. 4a and 7a). The other two gullies, though not as prominent but also blocked by talus, are marked as G1 and G3 (Figs. 4a and 7a). Therefore, ERT profiles D2–D6 were set up, crossing these gullies to reveal

Table 1 Characteristics of ERT acquisitions and of the inversion results

Profile	Number of electrodes	Spacing (m)	Max depth (m)	Iterations	RMS error (%)
D1	100	10	174	5	8.1
D2	86	10	146	5	3.4
D3	88	10	150	5	2.4
D4	52	10	86	5	4.1
D5	68	10	115	5	3.4
D6	88	10	136	5	10.5
D7	84	10	150	5	3.6
D8	68	10	115	5	6.1

Fig. 4 **a** Geomorphology map of the late Late Pleistocene Diexi gigantic landslide (black outline in Fig. 2). The position of the drilling holes according to Wang et al. (2014a, b); **b** cross-section along B-B' in Fig. 4a derived from the DEM
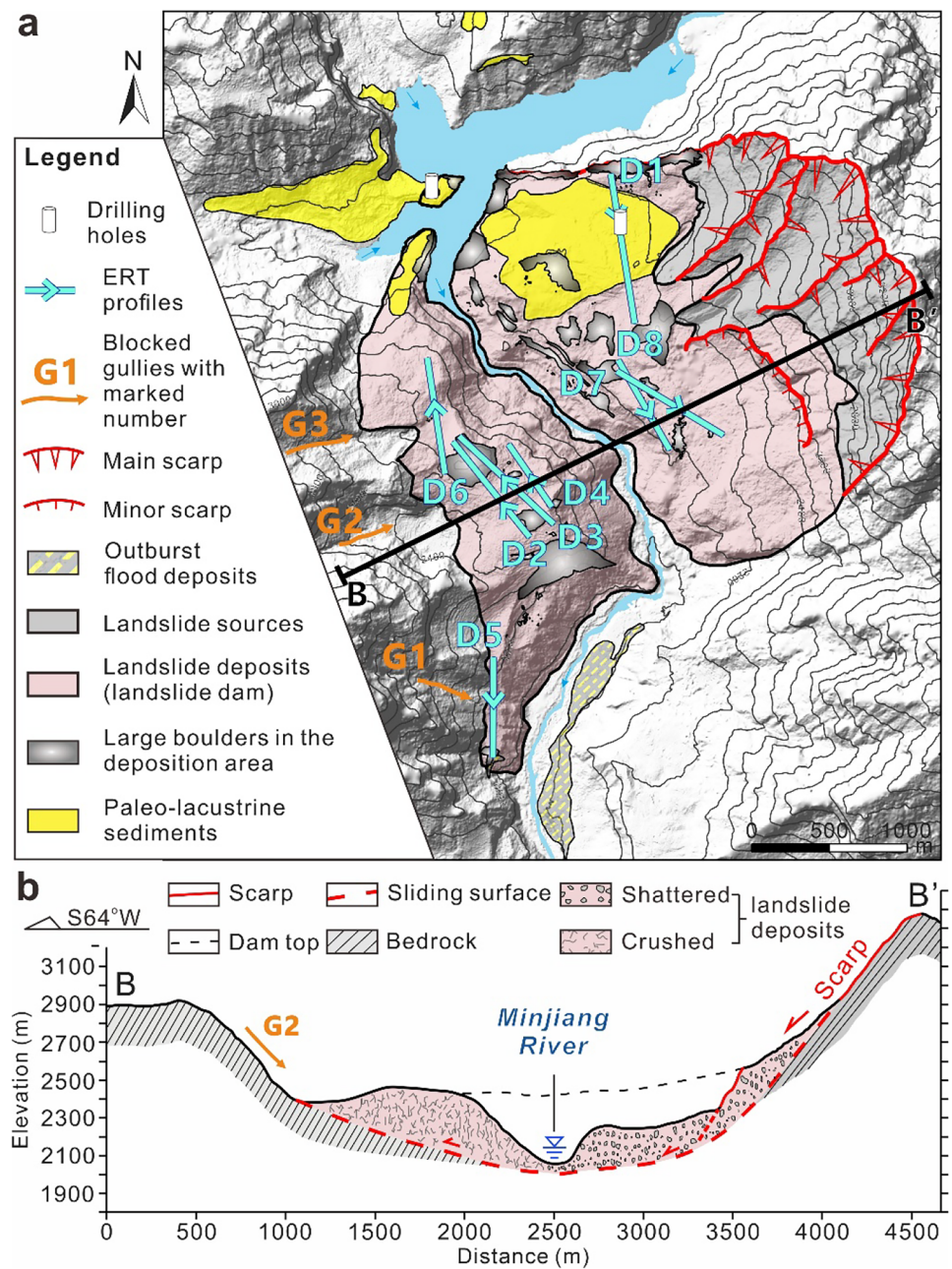
if they were blocked by the giant Diexi landslide. If so, we could further confirm the landslide boundary initially obtained by field geomorphic mapping.

The present surface morphology of the landslide dam is the result of erosional evolution for the past 30,000 years since its initial emplacement (see the cross section in Fig. 4b). It has been observed that the distal part of the dam does not undergo significant alteration compared to the proximal zone. The height of the dam at the distal portion is ~ 400 m from the current river bed, while the proximal zone has a height of only about 200 m. However, the erosional remnants of landslide deposits in the form

of crest lines have been particularly visible above 2490 m a.s.l. at the proximal location, indicating that the original topography has been extensively modified by intense linear erosion. Recently, Dai et al. (2021) pointed out that during the 1933 Diexi earthquake, the proximal part of the dam deposits experienced a mass sliding of ~ 21 million m³, and the distal and proximal side zone elevation was at the same level before this earthquake (Fig. 4b). The longitudinal analysis shows the downstream side of the dam is marked by steep slopes and higher elevations compared to the upstream side. It can be confirmed by the presence of thick lacustrine deposits on the proximal edge of the upstream area (Fig. 4a). The gentle

slopes on the landslide bodies are presently utilized for cultivation by the local people. The incised canyon formed by the lake outburst and lateral cutting of the landslide deposits produced a near-vertical slope on both sides of the river (Fig. 3c).

Through an extensive geological field survey, we found four types of materials in the deposition zone: (a) carapace (Davies and McSaveney 2004) with large boulders (Fig. 5a), which covers almost the entire surface of the landslide dam (Fig. 4a), apart from the absence of the southeast section due to the reactivation slip during the 1933 earthquake. Some of the boulders are more than 10 m in diameter. It is the most common sedimentary feature of large rock avalanches (Dufresne 2017). In our case, it is difficult for any other surface processes to produce such a wide distribution of large boulders, neither the intervention of human activities; (b) typical landslide deposition (Fig. 5b), located in the main landslide deposition body, characterized by large blocks supported with m-sized clasts and finer-grained materials. Large intact blocks were retained due to the limited movement distance and were generally found just below the carapace, especially outcrops on either side of the landslide flanks; (c) jigsaw-fractured false bedrock (Fig. 5c), located in the distal end of the landslide deposition, which looks like fractured bedrock, but actually is still part of the landslide deposition that remained and exhibiting the similar geological structure as original, pre-existing bedrock; (d) matrix facies formed by strong shearing and disintegration of the intact rock mass (Fig. 5d), which consist of highly fragmented debris in which grains of all sizes are mixed (typical of turbulent flow). Such sedimentary features were noted along the banks of deep canyons and ravines, alternating with more intact rock masses. Overall, the landslide deposits at the proximal side (close to the landslide scarp) are highly fragmented, while the distal side on the opposite bank of the river appears more intact, possibly due to the confined runout by the opposite hillslope (Fig. 4b). The locations of those photographs are shown in Fig. 3b.
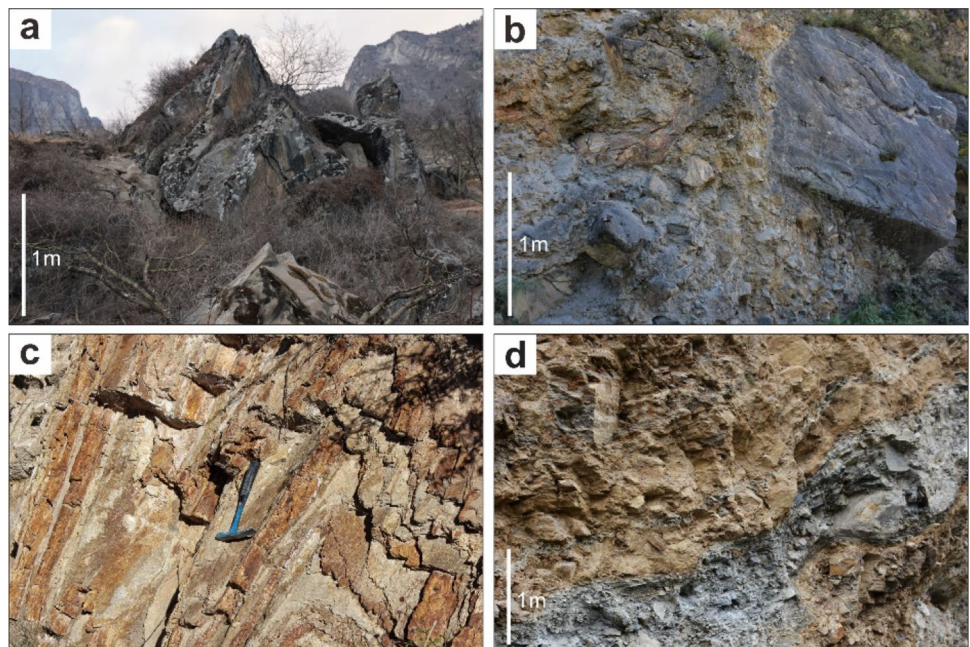
## The extent and characteristics of the Diexi paleo lake and lacustrine sediments

Field investigations were concentrated in an altitudinal bracket under 2500 m a.s.l. (dam crest) along the upstream reaches of the Minjiang River above the paleo-landslide dam crest to verify the remaining evidence of the paleo-lake shorelines and lacustrine sediments deposited in the lake that formed behind the paleo landslide dam. Using LiDAR-derived images, we clearly observed the shorelines from the surrounding terrain (Fig. 6a). In terms of lacustrine exposure investigation, close to the Zhengping Village, located ~ 26 km upstream from the dam site, we observed coarser grain size and turbidity current deposit features between lacustrine laminations (Fig. 6b), indicating that the transportation mode has changed from suspension to saltation (even traction), which infers that this site may have been the end of the paleo lake (Ma et al. 2022).

Altogether the authors documented 207 exposures of the lacustrine sediments in the field and reconstructed the areal extent of the paleo-lake with the highest elevation of 2390 m a.s.l. (Fig. 6c). The paleo-landslide dammed lake extended along both sides of the slopes and shortly intruded into the northeast Songping and Yuerzhai gullies by 5 km and 2 km, respectively, covering a total area of 21.4 km². Compared to the capacity of the dammed lake formed by the 1933 earthquake (Dai et al. 2021), the impact of the outburst floods is bound to be far-reaching (Ma et al. 2022). However, a more stable paleo-landslide dam body prevented the outbreak of floods from occurring in the short term.

Results of electrical resistivity profiles

Figure 7a shows the locations of eight ERT measurement profiles. The distribution of the diverse nature of landslide deposits with varying electrical properties made the interpretations very complex. The longest ERT profile D1, 1000 m long (Fig. 7b), located at

Fig. 5 a Carapace with large boulders; **b** typical landslide deposition characterized by large blocks supported with fine clasts; **c** jigsaw-fractured false bedrock; **d** matrix facies formed by strong shearing and disaggregating of the intact rock mass. The locations of these photographs are shown in Fig. 3b

Fig. 6 **a** Examples of shoreline segments of the paleo-lake; **b** lacustrine and fluvial sediments at the end of the paleo-lake; **c** estimated paleo-lake extent and exposures of the lacustrine sediments are represented by yellow dots, and the principal knickpoints are shown as white pentacles (Fan et al. 2019)
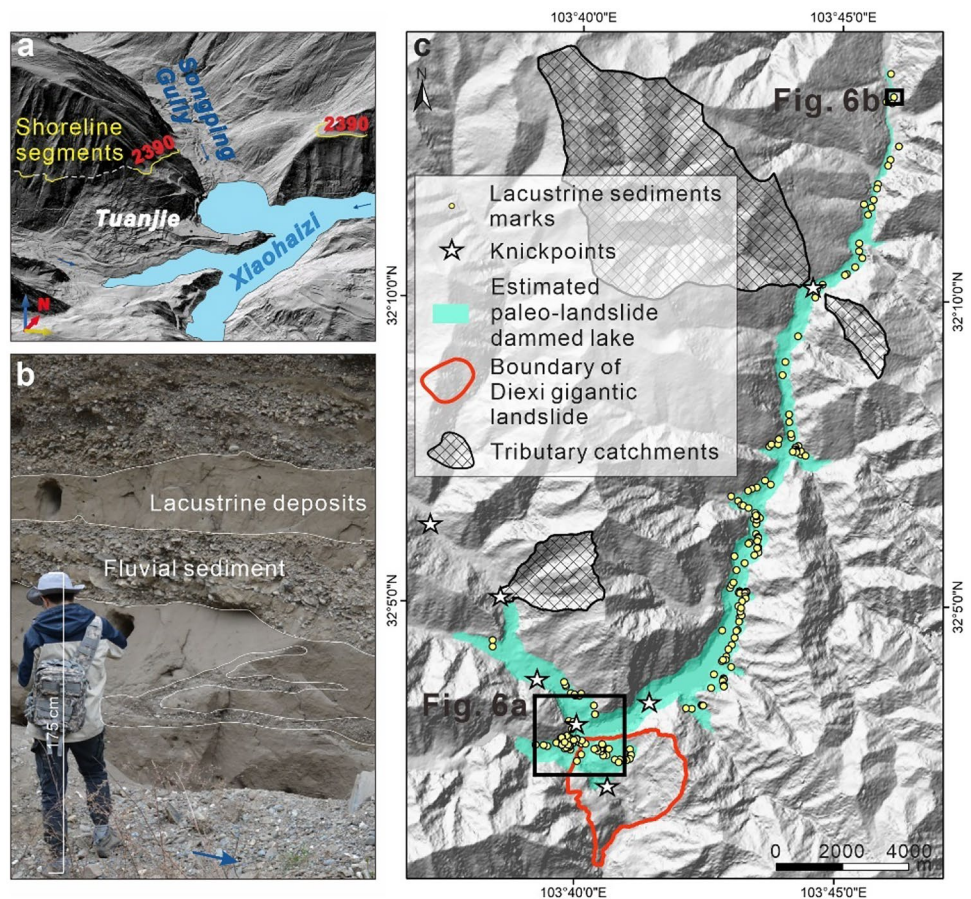
the Jiaochang platform, shows a wide distribution of superficial conductive layer L ($< 300\ \Omega$ m), 10 to 80 m thick. The thickness of layer L matches the borehole data at the same location (Fig. 7b; Wang et al. 2014b), which was advanced to a depth of 52 m, which included 49 m of lacustrine sediments. The distribution of the L layer is also consistent with the observed exposures of lacustrine sediments. The truncation of this layer appears to have been triggered by artificial excavation and landfill at the southern end, which is also reflected in the results summarized in Fig. 7b. Therefore, the continuation of L can be interpreted as a lacustrine plane and suggests that our imaging results are robust.

Figure 8 shows the resistivity profiles for D2 to D4 (distal end) near gully G2, oriented in the NNW-SSE, and consisting of three major electro-units. The 850-m-long D2 profile, located above the large gully G2 blocked by the rockslide deposits, is characterized by an average resistivity of 1500 Ω m. In this profile, we observe a sharp vertical lower resistivity body U ($< 300\ \Omega$ m) under gully G2, crossing 230 and between 460 m. The D2 profile has a maximum depth of 146 m, and this anomalously low resistivity layer extends beyond the maximum depth of investigation. The vertical contrast in resistivities might be the structure inside the rockslide deposits or because of the influence of surrounding bodies. The resistivity distribution in both flanks is more complex. In the northwest area, we observed a moderate resistivity body M (300 to 6000 Ω m). The rest of the resistivity model is occupied by multiple electro-units with relatively large resistivities, B ($> 6000\ \Omega$ m), with increasing

resistivities towards the southeastern and northwestern margins of the paleo slide feature. The northwestern end of the profile matches the location on top of the ridge.

We interpreted these three major electro-units as (i) blocky facies of intact typical of electro-unit B, (ii) matrix facies of sheared and disaggregated rocky materials for the electro-unit M, and (iii) loose, unconsolidated materials and crushed schists, weathered into clays, present groundwater flow, or a faulted margin of electro-unit U. Similar electro-units are also noticed in the other two profiles (D3 and D4) on the distal end. Although the D3 profile is located farther away from the ridge bordering the north side of the gully, the U and B units are on the Southeastern (S.E.). the side is prominent. The resistivity change might be due to material property changes within the deposits. Unit U is also shown on profile D4. However, it is observed that unit B in the Northwestern (N.W.) zone is thicker and more prominent, probably because of the higher elevation of D4, with the high resistivity portion located above the groundwater table. The higher resistivities are likely influenced by a higher coherence of the buried large block that is part of the deposits.

D5 and D6 profiles are located across the other two gullies, G1 and G3, which are downstream and upstream of the gully G2, respectively (Fig. 8). While most part of the D5 profile is still located on the rockslide materials. The low resistivity layer U1 ($< 300\ \Omega$ m) at the middle of the profile corresponds to the location of G1, indicating that the low resistivity material could be due to the presence

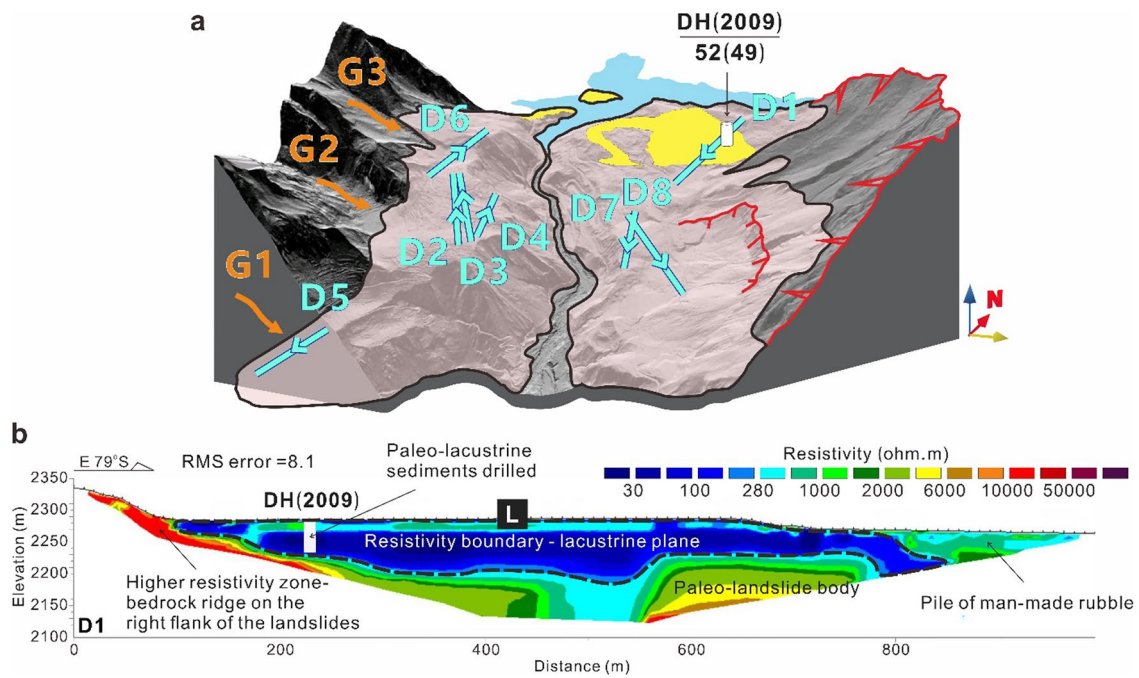**Fig. 7 a** Locations of geophysical survey profiles. The yellow area indicates the lacustrine deposit, which shows low resistivity on profile D1; geomorphic features are described in the legend of Fig. 4; **b** interpretation of the electric resistivity profile D1 with a detailed view of the formerly submerged part of the Diexi gigantic landslide deposits. D.H. (2009) is the location of the drilled borehole in 2009 (52-m total length including 49 m of lacustrine sediments, Wang et al. 2014b)

of colluvium deposited by G1 or the groundwater flow associated with G1. The Southwestern (S.W.) part of the resistivity model suggests a "high resistivity corner" I (>6000 Ω m), which indicates part of the southern end could be the in-situ "bedrock" units, lying beneath all of the landslide deposits. The D6 profile illustrates a very high resistivity layer O (>10,000 Ω m) over most of the profile. It overlays a superficial resistive layer with hundred Ω m resistivity (C). The lenticular conductive layer C consists of material filling gully G3, where the fine sediment only grew sod and broke away from the surrounding shrubby forest. It can be interpreted as the lake deposits or colluvium from G3, which do not belong to the rockslide itself and are not likely connected to the main lake because they could never have reached an altitude above 2400 m. The outcrops on the cliff wall below this profile clearly indicate that the high-resistivity materials (unit O) could represent highly coherent rock blocks within the deposits. Thus, the small lake could be formed by the rockslide blocking G3.

The resistivity profiles D7 (oriented in N.W.-S.E.) and D8 (N.N.W.-S.S.E.) are in the proximal part of the landslide (Fig. 9). The D7 profile exhibits a wide and relatively homogeneous distribution of a low-to-medium resistivity body H (~300 Ω m) within the subsurface, while the extension of H observed in the distal end is minimally visible at the D8 profile beneath the surface. These two profiles seem to be located on relatively homogeneous rockslide deposits that must include a significant component of fines that lower the overall resistivity. As aforementioned in the "Diexi landslide dam and present-day surface morphology" section, this portion of the landslide body has undergone considerable erosion

over time. Further, successive sediment deposition from the source area, along with the presence of gullies and cultivated land close to them, can contribute to low resistivity clusters. For example, in the D8 profile, the lower resistivity body G is located at depths below the ground level of 0–30 m; corresponding to this location, a gully is featured in the source region. On the other hand, the data show tiny high resistivity variations near the surface (T), located at depths below ground level between 0 and 10-m depth and confined at three separate locations in both D7 and D8 profiles. The field investigation confirmed the presence of very large boulders at these locations.

Due to some high contrasts induced by the complex subsurface inhomogeneities and the setup of the long array, three profiles (D1, D6, and D8) generate relatively high root mean square error (RMS), which is defined as the difference between the measured and calculated apparent resistivities. However, the inversion results of these ERT profiles are consistent with either the borehole data or the on-site geological observations, and thus, such analytical errors are acceptable and do not affect the robustness of the results.

Discussion

Anomalous resistivity zone
The most striking feature of the electrical resistivity tomography in the Diexi paleo landslide site is the presence of the vertical zone of anomalously low electrical resistivity (U) beneath the surface from profiles D2 to D4 extending to more than 150 m deep and about
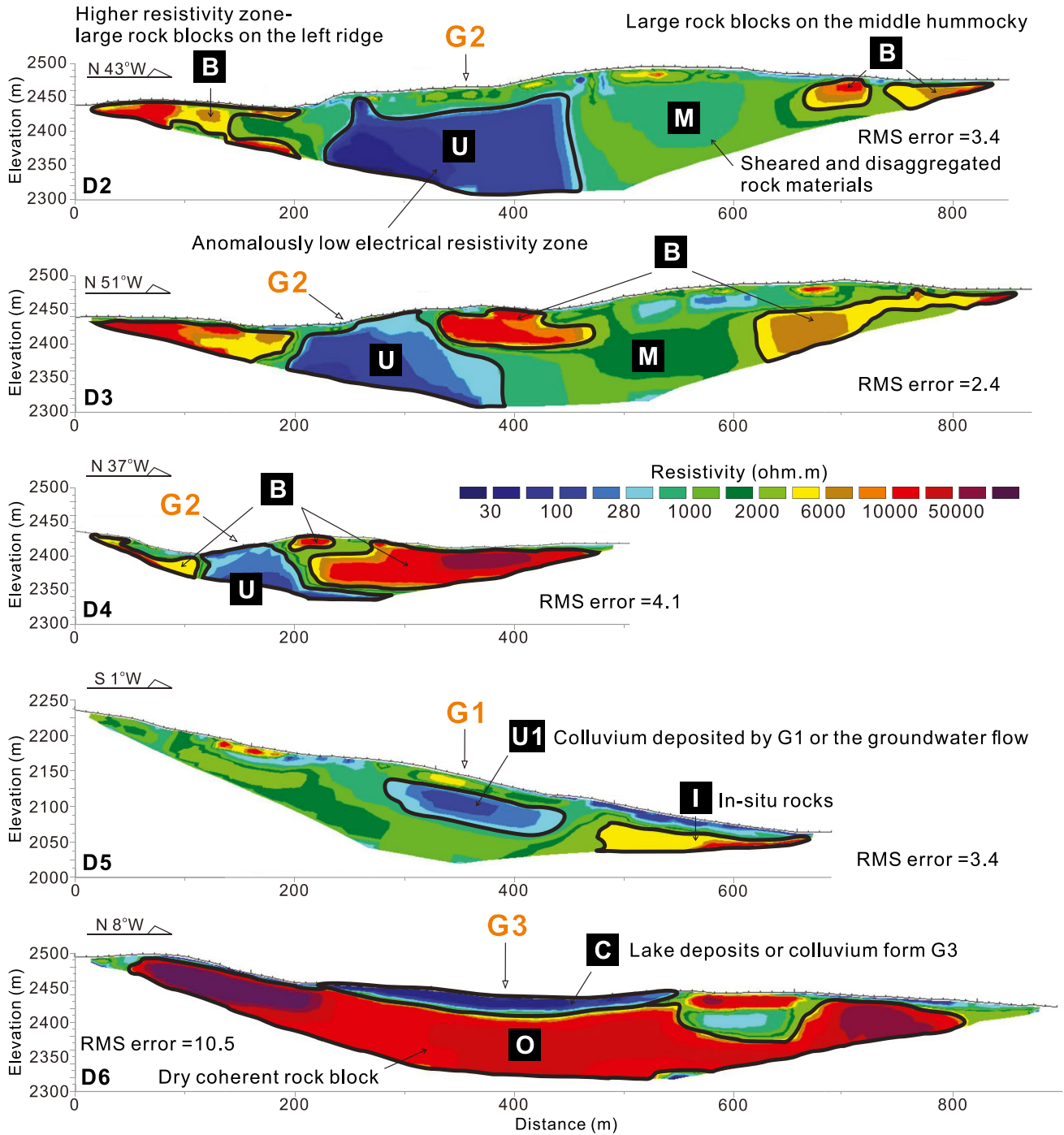
Fig. 8 Interpretation of the electric resistivity profiles D2 to D6 with a detailed view of the distal portion G1, G2, and G3 of the Diexi gigantic landslide deposit

300 m wide. This zone is outspreading from the distal end to the proximal zone with a decreasing trend. There are several possible candidates for interpreting such low resistivity zones:

(i)   Fault zone—concealed faults beneath the surface can induce low resistivities. Gélis et al. (2010) conducted a 2D ERT survey at the Experimental platform of Tournemire in France,

where there is a well-identified regional fault across the area, to detect the buried fault. Their results indicate that one of the low-resistivity discontinuities matches the location of the regional fault. Based on a 2D electrical resistivity tomography study, Arjwech et al. (2022) identified a suitable site for trenching, where there were no obvious morphotectonic features to locate the fault. However, in our study area, the
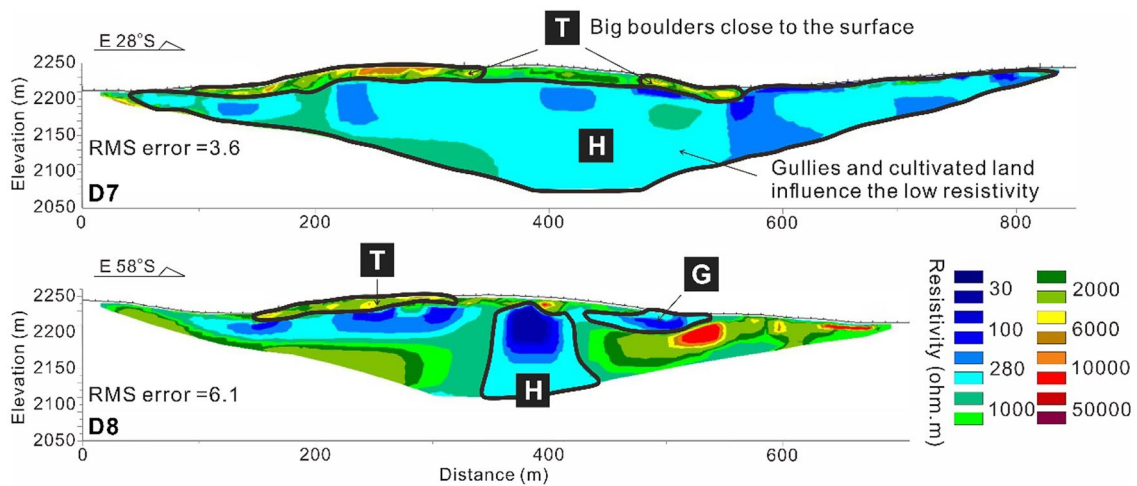
Fig. 9 Interpretation of the electric resistivity profiles D7 and D8 with a detailed view of the proximal portion of the Diexi gigantic landslide deposits

NNW-SSE ERT profile could only show clear fault contacts for NNE-SSW or NE-SW oriented structures, which are not known in this region. Strike-slip faults (e.g., Minjiang fault), like the one that most likely produced the 1933 Diexi earthquake, have an NNW-SSE orientation (Huang et al. 2003; Ren et al. 2018; Dai et al. 2021; Fig. 2), parallel with the ERT profile and thus unlikely to be detected by these resistivity profiles. Meanwhile, the Jiaochang structure comprises a series of Mesozoic folds and associated thrusts (Ren et al. 2018), and no evidence of tectonic activity in the last few tens of thousands of years has been presented yet. It is also possible to have a micro lineament deep under the burials. However, its extension did not show up to the D2 to D4 on the distal and D7 in the proximal zone (Figs. 8 and 9). Furthermore, available geological information, as well as extensive fieldwork, could not locate a fault morphotectonic landform/exposure within the Diexi paleo-landslide body.

(ii) Deposits with high clay content are another candidate for low subsurface resistivities (Unsworth et al. 1997). Sedimentary strata having thick phyllite and schist sequences are found in the source areas. Minerals in these rocks typically showcase higher clay content, and clays have low resistivities (Arjwech et al. 2021). Based on the high-resolution grain-size measurements, Liang and Jiang (2017) confirm that the Diexi lacustrine sediments have abundant clay. During the damming process, the soft sedimentary rocks may be crushed and transformed into fine clays.

(iii) A third possible candidate is the presence of fluids or saturation. Low resistivity values can be due to the presence of fluids in the deposits. Suzuki and Higashi (2001) observed that resistivity values decrease by up to 8% in highly porous and weathered rocks within a short period because of the heavy precipitation. During the summer rainfall months, water can be percolated through the weakly stratified landslide deposits inducing low resistivities. The water-saturated rocks or sediments through porous and permeable land-

fills via pore pressure buildup in the groundwater table or trapping water during damming could also induce very low resistivities (Urish 1981).

These aforementioned assumptions can partially explain the low resistivities in the ERT profiles. However, the confinement of the low values only to a narrow zone in the inversion of the ERT dataset suggests another component might be responsible for their origin. As resistivity largely depends on hydrogeological properties such as permeability (e.g., Priegnitz et al. 2015), porosity (e.g., Brunet et al. 2010), saturation (e.g., Wilkinson et al. 2010), infiltration (e.g., Looms et al. 2008), seepage (e.g., Sandberg et al. 2002), etc., understanding the effect of these factors on the ERT inversion results requires extensive detailing. In light of field evidence and interpretation of the ERT profiles, it can now be determined that the narrow stretch of the low resistivity sections (Fig. 8) corresponds with the large gully (G2) on the opposite side of the dam body. As mentioned in "The Diexi landslide dam and present-day surface morphology", this gully has a width of about 300 m and previously might have brought enough water from its large catchment area to the original Minjiang River. After the damming, water could have accumulated in this ditched portion. Because the dam fills consist of highly variable material properties, such coarse-grained zones are highly porous and permeable. Given the large gradient and catchment area, the potential for seepage and water saturation is highly possible through this gully (shown in Figs. 1 and 2).

Relation to dam breaching

The Diexi landslide is a consequent slope, sliding along the bedding. Its runout was halted by the opposite hillslope. Our ERT results and field investigations reveal that the dam body on the lake end consists of intact rocks. Landslide dams formed by such types of landslides normally have homogeneous material and can be consistently stable for an extended period by arresting pockets or seams of seepage and hydraulic piping.
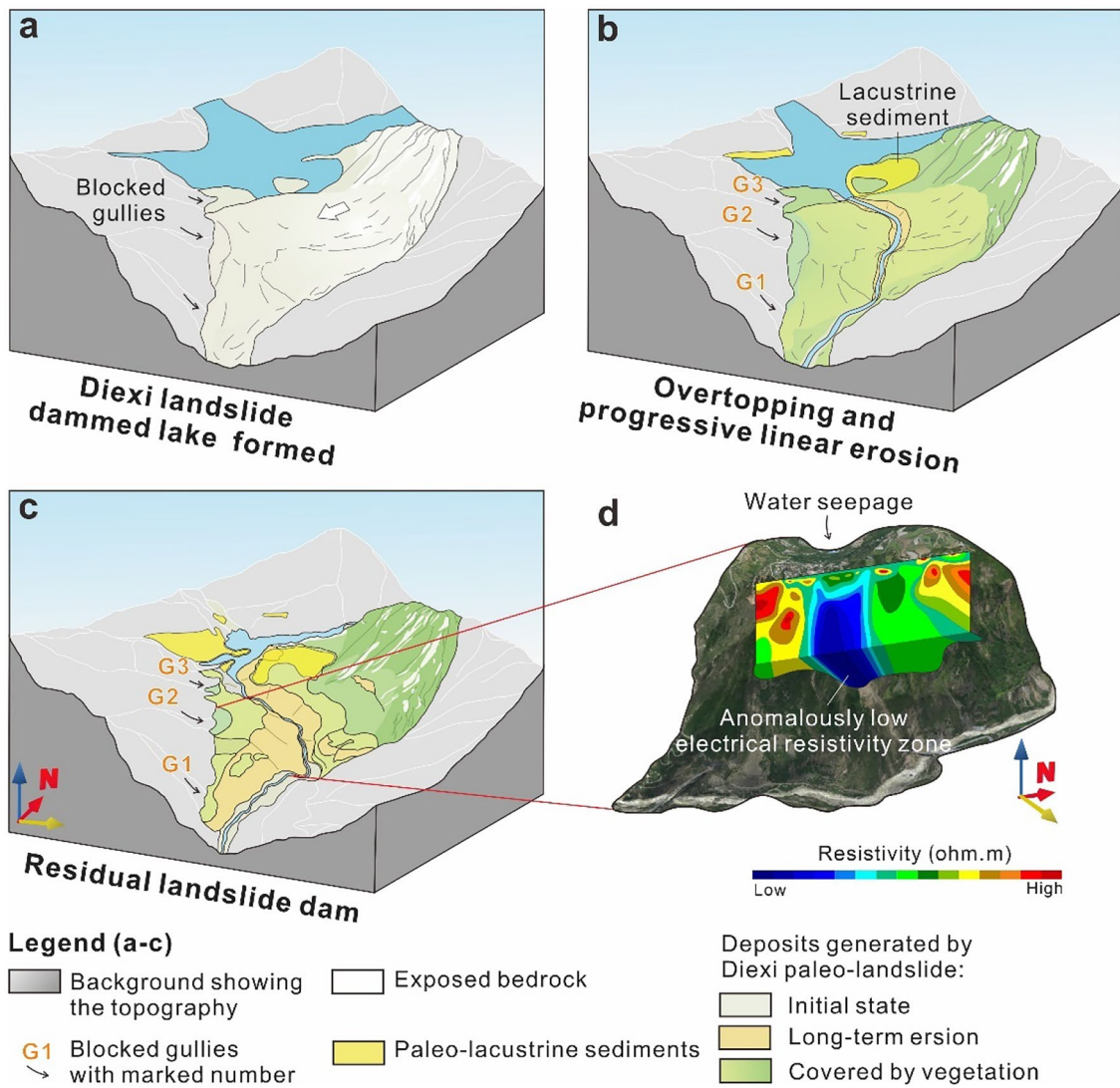
Fig. 10 Diagrams showing the dam failure mechanisms and sequences revealed by the ERT survey, remote sensing images, and field investigations. **a** The Diexi landslide blocked the Minjiang River and the gullies at the opposite side of the hillslope forming the landslide dam. The white arrows indicate the sliding direction. **b** Overtopping of the lake, causing strong linear erosion on top of the dam body. **c** The seepage from the wide and deep gully G2 may have weakened the dam body internally and eventually breached the dam. **d** The perspective diagrammatic of ERT units at G2 reveals deep and wide anomalously low electrical resistivity zone

In the Alpine belt, Films Sturztorm dammed the upper Rhine River valley, Switzerland, and breached about 8500 years after its formation (Wassmer et al. 2004) despite being double the size (10 km wide) of the Diexi landslide dam. Another perspective is that, in tectonically active areas like Diexi, earthquake shaking can trigger the collapse of dams, such as the one observed in the Mokihinui River dam collapse in New Zealand (Adams 1981). However, the analysis of disturbed layers in the lacustrine core sediments of Diexi lake revealed at least ten seismic incidents between 30,000 years B.P. and 15,000 years B.P. (Wang et al. 2014b, 2005). The stratigraphic record suggests that the dam was sufficiently stable to resist earthquake shaking during numerous events. Moreover, the seven terraces of fluvial deposits identified in the upstream location (Wang et al. 2014b) suggest that the breaching was likely by overtopping rather than seepage. But the high-resolution ERT result suggests that the weakest point in the landslide dam is the narrow, low-resistivity zone corresponding to the ditched gully G2 and the proximal downstream zone of the landslide dam. On the upstream side, the large coherent rock block within the subsurface revealed by both ERT and remote sensing images enhances the stability of the dam at G3 compared to the dam remnants at G2. It has also been evident from the geomorphic mapping (cf. "The Diexi landslide dam and present-day surface morphology") that flooding of the lake over the dam crest in the proximal areas produced strong linear erosion here. On the other hand, at the downstream side of G3, the large and ditched gully G2 perpendicular to the dam deposits could have allowed water seepage during heavy rainy periods that have been prolonged in the past. We postulate that the seepage from the gully G2 might have allowed the

already weak layers to weaken further, causing downcutting during overtopping flash flood seasons, finally breaching the Diexi dam and forming the present-day canyon morphology (Fig. 10).

Interpretation of ERT data presented here for the first time describes the internal structure of the Diexi paleo-landslide dam, which forms one of the longest stable landslide-dammed lakes in the geological literature. However, additional data are still needed to fully understand the likely breaching processes. Seismic surveys in the dam body can reveal the depth of low resistivity layers, as ERT measurements only reach a maximum depth of 150 m. Seismic surveys in the main dam body might also reveal the presence or absence of concealed faults to validate our hypothesis.

Conclusions

We present a comprehensive study on the longest-ever-lasted paleo landslide dam in Diexi, Sichuan, China, using geophysical techniques and extensive field investigations. With complementary geomorphology work using UAV's and LiDAR data, as well as field investigations of the dam and associated paleo-lakes, we provide valuable information on the breaching mechanisms of the paleo-dam. We image the subsurface structure of the paleo landslide dam in detail using the ERT technique. Eight ERT measurements with a maximum imaging depth of 174 m were carried out at both proximal and distal portions of the paleo-landslide deposits. The lake deposits are clearly imaged as low resistivity layers on the ERT profiles, and the thickness of the lacustrine deposits matches the drilling log. A prominent low-resistivity unit with a depth extent of more than 150 m and a width of about 300 m from the ERT profiles D2–D4 located near the gully G2 at the distal side of the landslide deposits indicates a possible zone of seepage associated with the pore water pressure migrating from the area of G2. Based on the interpreted results, we propose that breaching such a large paleo-landslide dam was not possible by overtopping alone. The geophysical and geomorphic evidence suggests that seepage from the surrounding gullies may have been caused by the downcutting, thus weakening the dam and eventually leading to its breaching. This study provides the first framework to understand the paleo-landslide dam using multiple modern investigation techniques, such as geophysical and geomorphic measurements, which are most effective when investigating paleo-landslide dams. Our results and conclusions provide valuable information for evaluating the internal stability of landslide dams in tectonically active regions.

Declarations

Conflict of interest The authors declare no competing interests.

References

Adams J (1981) Earthquake-dammed lakes in New Zealand. Geology 9:215–219. https://doi.org/10.1130/0091-7613(1981)9%3c215:ELINZ%3e2.0.CO;2

Alford, D., Schuster, R.L., (2000) Usoi landslide dam and Lake Sarez, an assessment of hazard and risk in the Pamir Mountains, Tajikistan. ISDR Prevention Series no. 1. Chap. 1

Arjwech R, Chaisuriya S, Rattanawannee J et al (2022) Recent paleoseismic investigations at the hidden Thakhek fault in Thailand. J Asian Earth Sci 236. https://doi.org/10.1016/j.jseaes.2022.105315

Arjwech R, Everett ME, Chaisuriya S et al (2021) Electrical resistivity tomographic detection of the hidden Thakek fault, Northeast Thailand. Near Surf Geophys 19:489–501. https://doi.org/10.1002/nsg.12165

Březný M, Pánek T, Braucher R et al (2021) Old but still active: > 18 ka history of rock slope failures affecting a flysch anticline. Landslides 18:89–104. https://doi.org/10.1007/s10346-020-01483-7

Brunet P, Clément R, Bouvier C (2010) Monitoring soil water content and deficit using Electrical Resistivity Tomography (ERT)—a case study in the Cevennes area, France. J Hydrol 380:146–153. https://doi.org/10.1016/j.jhydrol.2009.10.032

Burchfiel B, Zhiliang C, Yuping L, Royden L (1995) Tectonics of the Longmen Shan and Adjacent Regions, Central China. Int Geol Rev 37:661–735. https://doi.org/10.1080/00206819509465424

Chen CY, Chang JM (2016) Landslide dam formation susceptibility analysis based on geomorphic features. Landslides 13:1019–1033. https://doi.org/10.1007/s10346-015-0671-5

Chen S, Wilson CJL, Deng Q et al (1994) Active faulting and block movement associated with large earthquakes in the Min Shan and Longmen Mountains, northeastern Tibetan Plateau. J Geophys Res 99. https://doi.org/10.1029/94jb02132

Costa JE, Schuster RL (1991) Documented historical landslide dams from around the world. United States Geol Surv Open-File Rep 91–239:494

Dahlin T, Zhou B (2004) A numerical comparison of 2D resistivity imaging with 10 electrode arrays. Geophys Prospect 52:379–398. https://doi.org/10.1111/j.1365-2478.2004.00423.x

Dai L, Fan X, Jansen JD, Xu Q (2021) Landslides and fluvial response to landsliding induced by the 1933 Diexi earthquake, Minjiang River, eastern Tibetan Plateau. Landslides 18:3011–3025. https://doi.org/10.1007/s10346-021-01717-2

Davies TR, McSaveney MJ (2004) Dynamic fragmentation in landslides: application to natural dam stability. In: Evans SG, Strom AL (eds) Abstract volume, NATO advanced research workshop: security of natural and artificial rockslide dams. Kyrgyzstan, Bishkek, pp 7–13

Delunel R, Hantz D, Braucher R et al (2010) Surface exposure dating and geophysical prospecting of the Holocene Lauvitel rock slide (French Alps). Landslides 7:393–400. https://doi.org/10.1007/s10346-010-0221-0

Deng B, Liu S, Liu S et al (2013) Progressive Indosinian N-S deformation of the Jiaochang structure in the Songpan-Ganzi fold-belt, Western China. PLoS One 8:e76732. https://doi.org/10.1371/journal.pone.0076732

Dirks P, Wilson CJL, Chen S, Luo ZL, Liu S (1994) Tectonic evolution of the NE margin of the Tibetan Plateau; evidence from the central Longmen Mountains, Sichuan Province, China basement Indosinian intrusives 1: Xuelong bao granite. J Southeast Asian Earth Sci 9:181–192

Dong JJ, Tung YH, Chen CC et al (2009) Discriminant analysis of the geomorphic characteristics and stability of landslide dams. Geomorphology 110:162–171. https://doi.org/10.1016/j.geomorph.2009.04.004

Dufresne A, Ostermann M, Preusser F (2018) River-damming, late-Quaternary rockslides in the Ötz Valley region (Tyrol, Austria). Geomorphology 310:153–167

Dufresne A (2017) Rock avalanche sedimentology—recent progress. In: Advancing culture of living with landslides. Springer International Publishing, pp 117–122

Fan X, Dufresne A, Siva Subramanian S et al (2020) The formation and impact of landslide dams—state of the art. Earth-Science Rev 203:103116. https://doi.org/10.1016/j.earscirev.2020.103116

Fan X, Dufresne A, Whiteley J et al (2021) Recent technological and methodological advances for the investigation of landslide dams. Earth-Science Rev 218. https://doi.org/10.1016/j.earscirev.2021.103646

Fan X, Xu Q, Scaringi G et al (2017) Failure mechanism and kinematics of the deadly June 24th 2017 Xinmo landslide, Maoxian, Sichuan, China. Landslides 14. https://doi.org/10.1007/s10346-017-0907-7

Fan X, Yunus AP, Jansen JD et al (2019) Comment on 'Gigantic rockslides induced by fluvial incision in the Diexi area along the eastern margin of the Tibetan Plateau' by Zhao et al. (2019) Geomorphology. Geomorphology 338:27–42. https://doi.org/10.1016/j.geomorph.2019.106963

Gélis C, Revil A, Cushing ME et al (2010) Potential of electrical resistivity tomography to detect fault zones in limestone and argillaceous formations in the experimental platform of Tournemire, France. Pure Appl Geophys 167:1405–1418. https://doi.org/10.1007/s00024-010-0097-x

Havenith H-B, Bourdeau C (2010) Earthquake-induced landslide hazard in mountain regions: a review of case histories from Central Asia. Geol Belgica 13:135–150

Havenith HB, Torgoev I, Ischuk A (2018) Integrated geophysical-geological 3D model of the right-bank slope downstream from the Rogun dam construction site, Tajikistan. Int J Geophys 2018. https://doi.org/10.1155/2018/1641789

Hermanns RL, Hewitt K, Strom A, Evans SG, Dunning SA, Scarascia-Mugnozza G (2011) The classification of rockslide dams. In: Natural and artificial rockslide dams. Springer, pp 581–593

Hewitt K (1998) Catastrophic landslides and their effects on the Upper Indus streams, Karakoram Himalaya, northern Pakistan. Geomorphology 26:47–80. https://doi.org/10.1016/S0169-555X(98)00051-8

Hewitt K (2011) Rock avalanche dams on the Trans Himalayan upper Indus streams: a survey of late quaternary events and hazard-related characteristics. In: Natural and Artificial rockslide dams. Springer, pp 177–204

Høgaas F, Longva O (2019) The late-glacial ice-dammed lake Nedre Glomsjø in Mid-Norway: an open lake system succeeding an actively retreating ice sheet. Nor J Geol. https://doi.org/10.17850/njg98-4-08

Huang Z, Tang R, Li S (2003) Re-discussion on the Jiaochang Arcuate Structure, Sichuan Province, and the seismogenic structure for Diexi Earthquake in 1933. Earth Research in China 17.

Jiang H, Mao X, Xu H et al (2014) Provenance and earthquake signature of the last deglacial Xinmocun lacustrine sediments at Diexi, East Tibet. Geomorphology 204:518–531. https://doi.org/10.1016/j.geomorph.2013.08.032

King J, Loveday I, Schuster RL (1989) The 1985 Bairaman landslide dam and resulting debris flow, Papua New Guinea. Q J Eng Geol Hydrogeol 22(4):257–270

Kirby E, Reiners PW, Krol MA et al (2002) Late Cenozoic evolution of the eastern margin of the Tibetan Plateau: Inferences from 40Ar/39Ar and (U-th)/He thermochronology. Tectonics 21. https://doi.org/10.1029/2000tc001246

Kirby E, Whipple KX, Burchfiel BC, Berger G (2000) Quaternary deformation along the eastern margin of the Tibetan Plateau. America (NY) 375–393

Korup O (2002) Recent research on landslide dams—a literature review with special attention to New Zealand. Prog Phys Geogr 26:206–235. https://doi.org/10.1191/0309133302pp333ra

Korup O (2004) Geomorphometric characteristics of New Zealand landslide dams. Eng Geol 73:13–35. https://doi.org/10.1016/j.enggeo.2003.11.003

Korup O, Tweed F (2007) Ice, moraine, and landslide dams in mountainous terrain. Quat Sci Rev 26:3406–3422. https://doi.org/10.1016/j.quascirev.2007.10.012

Liang L, Jiang H (2017) Geochemical composition of the last deglacial lacustrine sediments in East Tibet and implications for provenance, weathering, and earthquake events. Quat Int 430:41–51. https://doi.org/10.1016/j.quaint.2015.07.037

Loke MH, Barker RD (1996) Rapid least-squares inversion of apparent resistivity pseudosections by a quasi-Newton method. Geophys Prospect 44:131–152. https://doi.org/10.1111/j.1365-2478.1996.tb00142.x

Looms MC, Jensen KH, Binley A, Nielsen L (2008) Monitoring unsaturated flow and transport using cross-borehole geophysical methods. Vadose Zone J 7:227–237. https://doi.org/10.2136/vzj2006.0129

Ma J, Chen J, Cui Z et al (2018) Sedimentary evidence of outburst deposits induced by the Diexi paleolandslide-dammed lake of the upper Minjiang River in China. Quat Int 464:460–481. https://doi.org/10.1016/j.quaint.2017.09.022

Ma J, Chen J, Cui Z et al (2022) Reconstruction of catastrophic outburst floods of the Diexi ancient landslide-dammed lake in the Upper Minjiang River, Eastern Tibetan Plateau. Springer Netherlands

Meric O, Garambois S, Jongmans D et al (2005) Application of geophysical methods for the investigation of the large gravitational mass movement of Séchilienne, France. Can Geotech J 42:1105–1115. https://doi.org/10.1139/t05-034

Pánek T, Hartvich F, Jankovská V et al (2014) Large Late Pleistocene landslides from the marginal slope of the Flysch Carpathians. Landslides 11:981–992. https://doi.org/10.1007/s10346-013-0463-8

Pánek T, Hradecký J, Minár J et al (2009) Late Holocene catastrophic slope collapse affected by deep-seated gravitational deformation in flysch: Ropice Mountain, Czech Republic. Geomorphology 103:414–429. https://doi.org/10.1016/j.geomorph.2008.07.012

Peng M, Zhang LM (2012) Breaching parameters of landslide dams. Landslides 9:13–31. https://doi.org/10.1007/s10346-011-0271-y

Perrone A, Lapenna V, Piscitelli S (2014) Electrical resistivity tomography technique for landslide investigation: a review. Earth-Science Rev 135:65–82. https://doi.org/10.1016/j.earscirev.2014.04.002

Priegnitz M, Thaler J, Spangenberg E et al (2015) Characterizing electrical properties and permeability changes of hydrate bearing sediments using ERT data. Geophys J Int 202:1599–1612. https://doi.org/10.1093/gji/ggv245

Qian H, Zhou R, Ma S, Li X (2000) South segment of Minjiang fault and Diexi earthquake in 1933. Earthq Res China 14(2):146–152

Ren J, Xu X, Zhang S et al (2018) Surface rupture of the 1933 M 7.5 Diexi earthquake in eastern Tibet: implications for seismogenic tectonics. Geophys J Int 212:1627–1644. https://doi.org/10.1093/gji/ggx498

Reneau SL, Dettier DP (1996) Late Pleistocene landslide-dammed lakes among the Rio Grande, White Rock Canyon, New Mexico. Geol Soc Am Bull 108:1492–1507

Sandberg SK, Slater LD, Versteeg R (2002) An integrated geophysical investigation of the hydrogeology of an anisotropic unconfined aquifer. J Hydrol 267:227–243. https://doi.org/10.1016/S0022-1694(02)00153-1

Santamarina JC, Rinaldi VA, Fratta D et al (2005) 4. A survey of elastic and electromagnetic properties of near-surface soils. Near-Surface Geophys 71–88. https://doi.org/10.1190/1.9781560801719.ch4

Shen D, Shi Z, Peng M et al (2020) Longevity analysis of landslide dams. Landslides 17:1797–1821. https://doi.org/10.1007/s10346-020-01386-7

Strom A (1998) Giant ancient rock slides and rock avalanches in the Tien Shan Mountains, Kyrgystan. Landslide News 11:20–23

Strom A (2010) Landslide dams in Central Asia region. J Japan Landslide Soc 47:309–324. https://doi.org/10.3313/jls.47.309

Suzuki K, Higashi S (2001) Groundwater flow after heavy rain in landslide-slope area from 2-D inversion of resistivity monitoring data. Geophys 66:733–743

Unsworth MJ, Malin PE, Egbert GD, Booker JR (1997) Internal structure of the San Andreas fault at Parkfield, California. Geology 25:359–362

Urish DW (1981) Electrical resistivity—hydraulic conductivity relationships in glacial outwash aquifers. Water Resour Res 17:1401–1408. https://doi.org/10.1029/WR017i005p01401

Wang E, Meng Q (2008) Discussion on the Mesozoic and Cenozoic tectonic evolution of the Longmen Shan fault belt. Science in China (Series D: Earth Sciences) 38(10):1221–1233 (in Chinese with English abstract)

Wang F, Dai Z, Okeke CAU et al (2018) Experimental study to identify premonitory factors of landslide dam failures. Eng Geol 232:123–134. https://doi.org/10.1016/j.enggeo.2017.11.020

Wang G, Furuya G, Zhang F et al (2016) Layered internal structure and breaching risk assessment of the Higashi-Takezawa landslide dam in Niigata, Japan. Geomorphology 267:48–58. https://doi.org/10.1016/j.geomorph.2016.05.021

Wang G, Huang R, Lourenço SDN, Kamai T (2014a) A large landslide triggered by the 2008 Wenchuan (M8.0) earthquake in Donghekou area: phenomena and mechanisms. Eng Geol 182:148–157. https://doi.org/10.1016/j.enggeo.2014.07.013

Wang L, Yang L, Wang X, Duan L (2005) Discovery of huge ancient dammed lake on upstream of Minjiang River in Sichuan, China. J Chengdu Univ Technol (Science & Technology Edition) 32(1):1–11 (in Chinese with English abstract)

Wang P, Zhang B, Qiu W, Wang J (2011) Soft-sediment deformation structures from the Diexi paleo-dammed lakes in the upper reaches of the Minjiang River, east Tibet. J Asian Earth Sci 40:865–872. https://doi.org/10.1016/j.jseaes.2010.04.006

Wang XQ, Li YR, Yuan Y et al (2014b) Palaeoclimate and palaeoseismic events discovered in Diexi barrier lake on the Minjiang River, China. Nat Hazards Earth Syst Sci 14:2069–2078. https://doi.org/10.5194/nhess-14-2069-2014

Wassmer P, Schneider JL, Pollet N, Schmitter-Voirin C (2004) Effects of the internal structure of a rock-avalanche dam on the drainage mechanism of its impoundment, Flims sturzstrom and Ilanz paleo-lake, Swiss Alps. Geomorphology. https://doi.org/10.1016/j.geomorph.2003.11.003

Wayne WJ (1999) The Alemania rockfall dam: a record of a mid-Holocene earthquake and catastrophic flood in northwestern Argentina. Geomorphology 27:295–306. https://doi.org/10.1016/S0169-555X(98)00080-4

Whiteley JS, Chambers JE, Uhlemann S et al (2019) Geophysical monitoring of moisture-induced landslides: a review. Rev Geophys 57:106–145. https://doi.org/10.1029/2018RG000603

Wilkinson PB, Chambers JE, Meldrum PI, Gunn DA, Ogilvy RD, Kuras O (2010) Predicting the movements of permanently installed electrodes on an active landslide using timelapse geoelectrical resistivity data only. Geophys J Int 183:543–556

Xu H, Chen J, Cui Z, Chen R (2020) Sedimentary facies and depositional processes of the Diexi Ancient Dammed Lake, Upper Minjiang River, China. Sediment Geol 398:105583. https://doi.org/10.1016/j.sedgeo.2019.105583

Xu H, Jiang H, Yu S et al (2015) OSL and pollen concentrate 14C dating of dammed lake sediments at Maoxian, east Tibet, and implications for two historical earthquakes in AD 638 and 952. Quat Int 371:290–299. https://doi.org/10.1016/j.quaint.2014.09.045

Yang W, Zhu L, Zheng H et al (2008) Evolution of a dammed paleolake in the Quaternary Diexi basin in the upper reaches of the Minjiang River, Sichuan, China. Geol Bull China 27:605–610 (in Chinese with English abstract)

Yılmaz S, Narman C (2015) 2-D electrical resistivity imaging for investigating an active landslide along a ridgeway in Burdur region, southern Turkey. Arab J Geosci 8:3343–3349

Zhang HP, Liu SF, Yang N et al (2006) Geomorphic characteristics of the Minjiang drainage basin (eastern Tibetan Plateau) and its tectonic implications: new insights from a digital elevation model study. Isl Arc 15:239–250. https://doi.org/10.1111/j.1440-1738.2006.00524.x

Zhong N, Jiang H, Haibing LI et al (2019) Last deglacial soft–sediment deformation at Shawan on the eastern Tibetan plateau and implications for deformation processes and seismic magnitudes. Acta Geol Sin 93:430–450. https://doi.org/10.1111/1755-6724.13773

Lanxin Dai · Xuanmei Fan (✉) · Dan Wang · Ali P. Yunus · Srikrishnan Siva Subramanian
State Key Laboratory of Geohazard Prevention and Geoenvironment Protection, Chengdu University of Technology, Chengdu 610059, People's Republic of China
Email: fxm_cdut@qq.com

Fanyu Zhang
MOE Key Laboratory of Mechanics on Disaster and Environment in Western China, and Department of Geological Engineering, Lanzhou University, Lanzhou 730000, People's Republic of China

J. David Rogers
Geological Engineering Program, Missouri University of Science and Technology, Rolla, MO 65409, USA

Hans-Balder Havenith
Geohazards and Environment, Department of Geology, University of Liege, Liege 4000, Belgium